Journal of Applied Electrochemistry **29**: 627–635, 1999.

Large specific surface area nanocrystalline Ti–Ru–Fe cathode materials for sodium chlorate

H. RAZAFITRIMO[1], M. BLOUIN[1], L. ROUÉ[1], D. GUAY[1]*, J. HUOT[2] and R. SCHULZ[2]
[1]*INRS-Énergie et Matériaux, 1650 Blvd Lionel-Boulet, C.P. 1020, Varennes, Québec, Canada J3X 1S2;*
[2]*Institut de Recherche d'Hydro-Québec, 1800 Blvd Lionel-Boulet, C.P. 1000, Varennes, Québec, Canada J3X 1S1*
*(*author for correspondence)*

Received 5 June 1998; accepted in revised form 11 November 1998

Key words: ball-milling, electrocatalyst, hydrogen evolution, leaching, lixiviation, nanocrystalline alloys, sodium chlorate

Abstract

Ball-milled nanocrystalline Ti_3RuFe powders were mixed with 1, 2, 4, 10 and 20 equivalents of Al and the mixtures were milled again for 20 h. The amount of Al atoms dissolved into the B2 structure of Ti_3RuFe does not exceed 8–9 at %, the remaining being present as elemental Al into the powder mixture. During a subsequent treatment of the composite powder in alkaline solutions, the elemental Al is leached out, while Al solutes in the B2 structure are not affected. An examination of the surface by scanning electron microscopy reveals that the leached powder has a highly porous surface structure. Surface area measurements performed by BET measurements show that there is a tenfold increase in the effective surface area. Activated electrodes made from these porous materials show a significant decrease of the cathodic overpotential for hydrogen evolution in typical chlorate electrolysis conditions of about 80 mV.

1. Introduction

The electrolysis of aqueous alkali chlorides, the first step in the process of sodium chlorate formation, is plagued with a high overpotential. About 90% of this overpotential comes from the cathodic side of the reaction, where hydrogen evolution occurs as the counter reaction. Typically, the cathodic overpotential for the mild steel cathodes used in the industry is of the order of 900 mV in typical chlorate electrolysis conditions. A reduction of this overpotential value by 300 mV would cause at least a 10% decrease in the energy consumption at the electrolysis step. Obviously, important energy savings could be obtained by developing efficient activated cathodes for this process.

Nanocrystalline materials [1] have demonstrated very interesting properties, often quite different from usual polycrystalline alloys. This is believed to be due to the high ratio of surface atoms over bulk atoms, which can be as high as 50% when crystal size is less than 5 nm. In the field of electrochemistry, nanocrystalline Ni [2] and Ru [3] have shown higher corrosion resistance than their polycrystalline counterparts. Elsewhere, it was demonstrated that nanocrystalline Ni–Mo–O activated cathodes show superior electrocatalytic activities for hydrogen evolution in alkaline solutions [4, 5]. Clearly, nanocrystalline materials are becoming an important class of materials whose electrochemical properties are of great interest.

There are several ways to prepare nanostructured materials like the evaporation–condensation technique [6] or the heat treatment of some amorphous alloys [7, 8]. Mechanical attrition is also an interesting alternative [9], since it allows the preparation of metastable nanocrystalline alloys of various compositions in quantities large enough to fulfill the requirement of mass production. In high energy ball-milling, numerous ball–powder–ball and ball–powder–container collisions occur, leading to repeated fractures and welding of particles. The mechanical deformations create numerous structural defects, increase the interdiffusion between alloying elements at interfaces of welded particles, and

cause the reduction of the size of crystallites to the nanometer range.

We have recently prepared nanocrystalline Ti–Ru–Fe–O alloys by high energy ball-milling, and have used these materials to fabricate activated cathodes for the electrolysis of sodium chlorate [10–12]. In typical chlorate electrolysis conditions, the best performing activated cathode exhibits an overpotential 250–300 mV lower than that of steel cathodes which are, at the present time, commonly used in the industry.

Any increase of the activity of an electrode material can be due to intrinsic and/or extrinsic factors. A corollary to this observation is that, given a certain level of intrinsic activity of a material, it will always be advantageous to increase the effective surface area of the solid–liquid interface. This well-known phenomenon is at the heart of Raney nickel-based electrodes, which are among the best activated cathodes for hydrogen evolution in basic solution. In Raney Ni, the modest intrinsic activity of Ni is compensated by a very large specific surface area.

Raney-type materials can be obtained by first preparing a two components system (XY), where X is the electrode material of which one is interested to increase the effective surface area, and Y is a leachable element. In a second step, Y is removed from the two components system, leaving a highly porous surface. In the case of Raney Ni, X stands for Ni, and highly porous Raney Ni have been prepared from Ni–Al alloys. Raney Ni can also be obtained by sherardization of Ni electrodes, that is reaction of Ni with Zn vapour to form an alloy, with subsequent leaching in caustic solution [13]. Likewise, sulfidation of Ni electrodes with hydrogen sulfide produces nickel sulfide which can then be reduced during cathodic hydrogen evolution, leaving a porous substrate behind [13].

It would be of great technological importance to be able to increase the effective surface area of more complex system where X is composed of several elements. For example, we have shown recently [10] that milling of $2Ti + 1Ru + 1Fe$ leads to the formation of a metastable simple cubic phase (Ti_2RuFe) highly active for H_2 discharge in typical chlorate electrolysis conditions. Increasing the effective surface area of this nanocrystalline alloy, which is typically of about 1 $m^2\ g^{-1}$, possibly would lead to still further reduction of the cathodic overpotential. This can only be done if an appropriate way to prepare the XY component system without causing an irreversible transformation of the metastable and active phase can be found.

Recently, we have used high energy ball-milling to prepare nanocrystalline materials containing one element that can be selectively removed to produce highly porous metastable structures [14]. This procedure was used to increase the effective surface area of hydrogen storage compounds and improve the hydriding and dehydriding kinetics [15]. In this paper, a similar approach was retained and the high energy ball-milling and leaching techniques were used to prepare porous nanocrystalline Ti–Ru–Fe alloys. As prepared nanocrystalline Ti–Ru–Fe (3:1:1 ratio) was milled with Al for different periods of time and with different Al concentrations. The structure and morphology of the powder at selected steps of the manufacturing process was determined. In typical chlorate electrolysis conditions these porous materials shows about 80 mV reduction of the cathodic overpotential for hydrogen evolution as compared with cathodes made of nonporous nanocrystalline alloys.

2. Experimental details

2.1. *Powder preparation*

Nanocrystalline alloys of Ti–Ru–Fe (3:1:1) and powder mixtures with Al were prepared by high energy ball-milling. The mechanical alloying was performed with a SPEX 8000 laboratory ball-mill, using a steel crucible (length of 47.6 mm and diameter of 38.1 mm) and three hardened steel balls (one of 14.3 mm diameter and two of 11 mm diameter). Ti (99.5%), Ru (99.95%), Fe (99.9%), and Al (99.9%) powders were used as starting materials. Nanocrystalline Ti–Ru–Fe (3:1:1) powders were obtained from milling the appropriate ratio of Ti, Ru and Fe for 40 h. Once the alloy was formed, various amounts of Al were introduced in the crucible and the mixtures were milled for an other 20 h (unless specified otherwise) to yield Ti:Ru:Fe:Al (3:1:1:x). The charge of the crucible was 5 g in all cases to keep the ball to powder weight ratio close to 4.5:1. The loading and the sampling of the powders were performed in a glove box under argon atmosphere. The crucible was kept sealed with a viton O-ring during milling.

The leaching was performed at ambient temperature with a 1 N NaOH solution in an ultrasonic bath. At the beginning, strong gas evolution occurred. After 2 h of leaching, the samples were washed with deionized water and dried overnight in an oven at 50 °C.

2.2. *Powder characterization*

X-ray diffraction studies were conducted with a Philips PW3040 X-ray diffractometer using Cu$K\alpha$ radiation. Structural information was obtained from the XRD spectra by Rietveld refinement analysis, performed by

using Rietan-94 software [16, 17]. All XRD patterns shown herein were Fourier filtered. Scanning electron microscopy (SEM) and energy dispersive X-ray (EDX) analysis were performed on a HITACHI S-570 microscope to reveal the composition and microstructure of the powders. An Altamira Instrument AMI1 was used to evaluate the specific surface areas by the Brunauer–Emmet–Teller (BET) method.

2.3. *Electrode preparation*

The working electrodes were made by cold pressing the milled or the leached powder. A stainless steel dye of 1.59 cm diameter was used to press the powder with a load of 20 000 kg cm^{-2} during 10 min. The pressed pellet was mounted at the end of a glass tube with an epoxy resin. The electrical contact was made by an electrical wire glued on the back of the disc by a silver paint.

2.4. *Electrochemical measurements*

A potentiostat–galvanostat (EG&G, model 273A) controlled by CorrWare software was used for all electrochemical measurements. These were made at 70 °C and in an electrolyte containing 550 g l^{-1} $NaClO_3$, 110 g l^{-1} NaCl, 1 g l^{-1} NaClO and 3 g l^{-1} $Na_2Cr_2O_7$ at pH 6.5. Only the front surface of the working electrode was exposed to the electrolyte. The electrode system consisted of a working electrode, a counter electrode (Pt) and a saturated calomel electrode (SCE) as reference. The activity of the electrodes was determined in galvanostatic mode, by recording the time evolution of the electrode potential at an applied current density of 250 mA cm^2. All electrode potentials have been corrected for the ohmic drop using the current interrupt technique. In some cases, the value of the uncompensated resistance was evaluated by impedance spectroscopy measurements using a Solartron frequence response analyser (SI 1255). Potentials are given with respect to the SCE reference.

3. Results and discussion

3.1. *Structure and composition before leaching*

We present in Figure 1, curve (a), the XRD spectrum of as ball-milled nanocrystalline Ti–Ru–Fe (elemental ratio 3:1:1). The spectrum exhibits the characteristic diffraction lines of a B2 structure (cP2–CsCl). Addition of one equivalent of Al to this alloy (nominal composition Ti–Ru–Fe–Al (3:1:1:1)) and further milling causes the appearance of new features in the XRD pattern. The X-ray peaks of Al disappear rapidly as a result of particle size reduction and dissolution of Al atoms into the Ti–Ru–Fe cubic structure. Also, a gradual shift of the X-ray peaks of the cubic phase toward larger angles is observed. For milling times exceeding 10 h, no further change is observed in the XRD patterns. The XRD pattern of the powder obtained after 40 h of milling is shown as a representative example in Figure 1, curve (b).

It has been shown elsewhere that the milling of an elemental mixture of Ti:Ru:Fe (2:1:1) leads to the formation of nanocrystalline cubic Ti_2RuFe (cP2–CsCl) [10]. In its ordered form, Ti atoms occupy the 1a site of the unit cell, while both Ru and Fe atoms fill the 1b site randomly. The fact that the XRD pattern of Ti_3RuFe (Figure 1) resembles that of Ti_2RuFe indicates that both compounds have a similar structure. Ti_2RuFe is formed by dissolution of Ru and Fe into hcp Ti, which transforms to β-Ti (cubic structure). Partial ordering of Ti on the 1a site and of Ru and Fe on the 1b site occurs with increasing Ru and Fe content, leading eventually to the formation of Ti_2RuFe [10]. The same mechanism applies in the case of Ti_3RuFe. The diffraction peaks in Figure 1 have a width comparable to that of nanocrystalline of Ti_2RuFe [10], indicating that the crystallites are of the same size (about 8–10 nm).

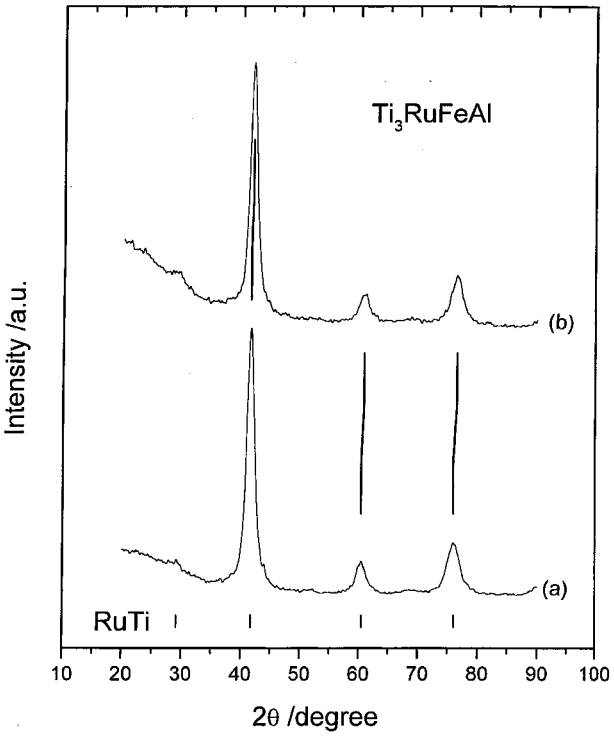

Fig. 1. XRD patterns of (a) Ti–Ru–Fe (3:1:1) milled 40 h and (b) Ti–Ru–Fe–Al (3:1:1:1) after an additional 40 h of milling. Positions of the diffraction peaks of cubic RuTi are shown at bottom.

Rietveld analyses of the XRD spectra after the addition of Al were performed to extract the lattice parameters of the cubic phase as a function of the milling time (Fig. 2). During the first 10 h of milling with Al, there is a steady decrease of the lattice parameter from about 3.062 Å to 3.050 Å. Considering that the covalent radius of Ti, Ru, Fe and Al are 1.32, 1.25, 1.17 and 1.18 Å, respectively, the decrease of the lattice parameter with time indicates the dissolution of Al into the B2 structure during milling. This process is relatively fast since no significant variation of the lattice parameter is observed after 10 hours of milling.

Mixtures of nanocrystalline Ti:Ru:Fe (3:1:1) with various Al contents were also milled for 20 h (Figure 3). The main spectral features are similar to that of the parent alloy, except for some extra peaks which belong to Ti oxide phases. The presence of elemental Al in the powder manifests itself by the occurrence of very broad diffraction peaks located at about 38.5 and about 45°, on both sides of the main (1 1 0) diffraction peak of the cubic phase.

The variation of the lattice parameter of the cubic phase with Al content is displayed in Figure 4. The lattice parameter, a, decreases from 3.06 Å for the Al free alloy to 3.025 Å when $x = 4$. An estimate of the amount of Al in the B2 structure could be obtained from the variation of the lattice parameter using Vergard's law, but in the case of Ti–Al not much structural data

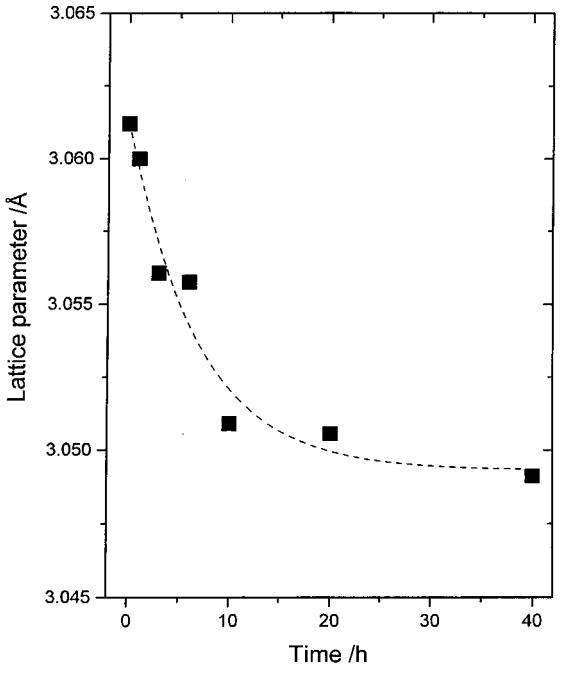

Fig. 2. Variation of the lattice parameter of the cubic phase with respect to milling time for Ti:Ru:Fe:Al (3:1:1:1).

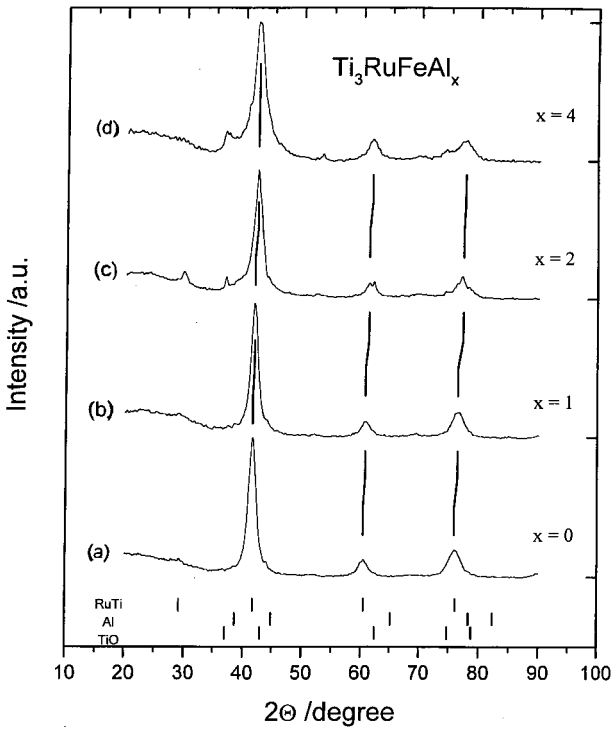

Fig. 3. XRD patterns of (a) Ti–Ru–Fe (3:1:1) milled 40 h, and after an additional 20 h of milling with Al (Ti–Ru–Fe–Al (3:1:1:x)), (b) $x = 1$, (c) $x = 2$ and (d) $x = 4$.

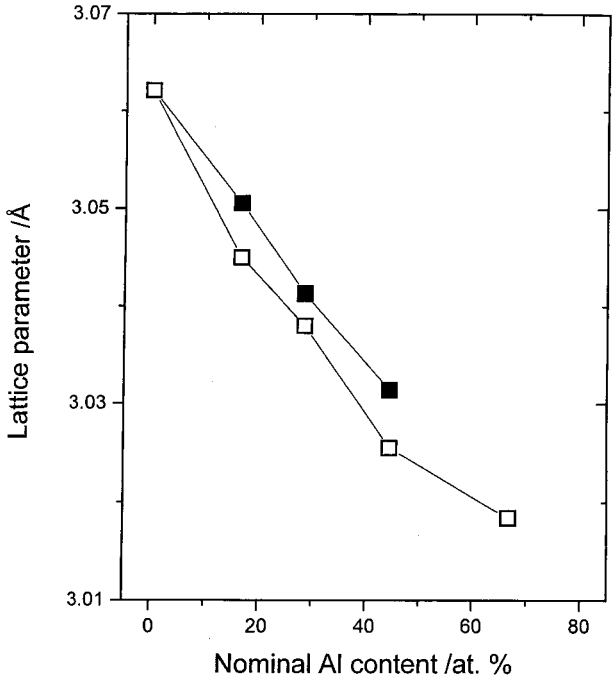

Fig. 4. Variation of the lattice parameter of the B2 structure with respect to the nominal Al content added to Ti_3RuFe. The milling operation was resumed for an additional 20 h after the addition of Al. Key: (■) before leaching; (□) after leaching.

are available on cubic β-Ti(Al). As shown by McCullough [18], the high-temperature β-Ti(Al) phase cannot be retained upon quenching. It transforms to the hexagonal α-phase. Also, to our knowledge, β-Ti(Al) does not form upon milling. Instead, a hcp α-Ti(Al) or fcc phase forms depending on the Ti/Al ratio [19, 20–23]. So, considering that the covalent radius of Al is almost identical to that of Fe, we will assume in a first approximation that the effect of Al on the lattice parameter of β-Ti is identical to that of Fe.

We present in Figure 5, the variation of the lattice parameter of β-Ti as a function of the Ru and Fe content. The solubility of Fe in β-Ti (data points □) presents an upper limit at 21 at % Fe. This limit can be extended by rapid quenching. Ray et al. [24] showed that the lattice parameter of the cubic phase at the equiatomic composition TiFe lies on the same straight line (data point ■). Zaluski et al. [25] have shown that the variation of the lattice parameter of ball-milled Ti(Fe) also follows the results of Ray et al. A similar relationship exists between the lattice parameter of β-Ti (Ru) (data points ○) and the parameter of the equiatomic RuTi compound (data point ●). With the above assumptions and upon application of the Vergard's law, the lattice parameter of Ti_3Ru Fe should be 3.063 Å (point (a) in Fig. 5). This value is close to what we find experimentally, 3.061 Å (first point in Fig. 2). Along the same line, the lattice parameter $a = 3.050$ Å obtained after extensive milling of a mixture of Ti:Ru:Fe:Al with the ratio (3:1:1:1) corresponds to a Ru + Fe + Al total content of 42.4 at % (see point (b) in Fig. 5) and thus 2.4 at % of Al in the cubic structure. Finally, when a large excess of Al is milled with Ti_3RuFe, the lattice parameter reaches 3.018 Å (see Fig. 4). That corresponds to a Ru + Fe + Al content of 48.2 at %, or an Al content of 8.2 at %, in the B2 structure (point (c) in Fig. 5).

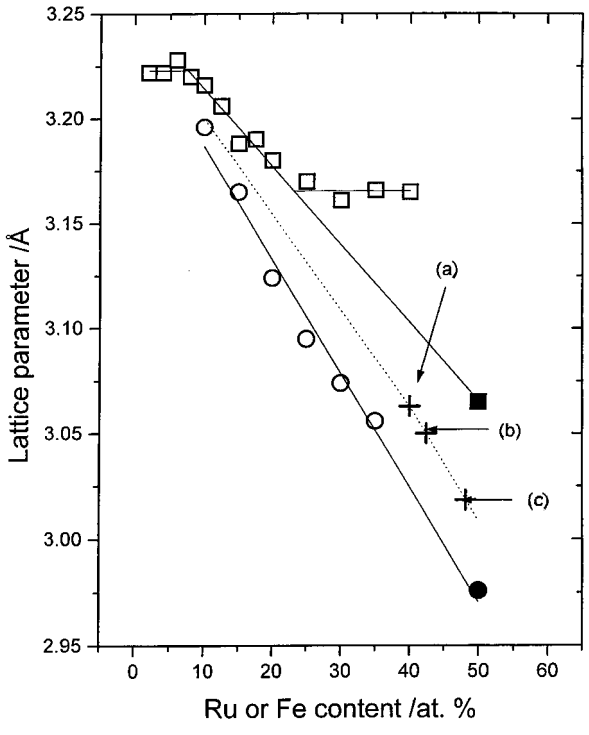

Fig. 5. Variation of the lattice parameter of (○) β-Ti(Fe) [24] and (□) β-Ti(Ru) [31] with respect to iron and ruthenium content. The lattice parameters of equiatomic (●) TiFe and (■) RuTi are also presented. The dotted line represents the variation of the lattice parameter with Fe, Ru and Al into the B2 structure. The meaning of the data points (a), (b) and (c) is given in the text.

3.2. *Structure and composition after leaching*

The composition of the powder before and after leaching was monitored by EDX analysis. In all cases, the Ti, Ru and Fe were found to be in the ratio 3:1:1. The Al content of the powder before and after leaching is presented in Figure 6 as a function of the nominal Al composition. Error bars take into account the spatial inhomogeneity observed between larger and smaller grains. Before leaching, the measured Al content is overestimated, probably because of the excess Al on grain surfaces and interfaces. After leaching, only a small amount of Al remains in the powder.

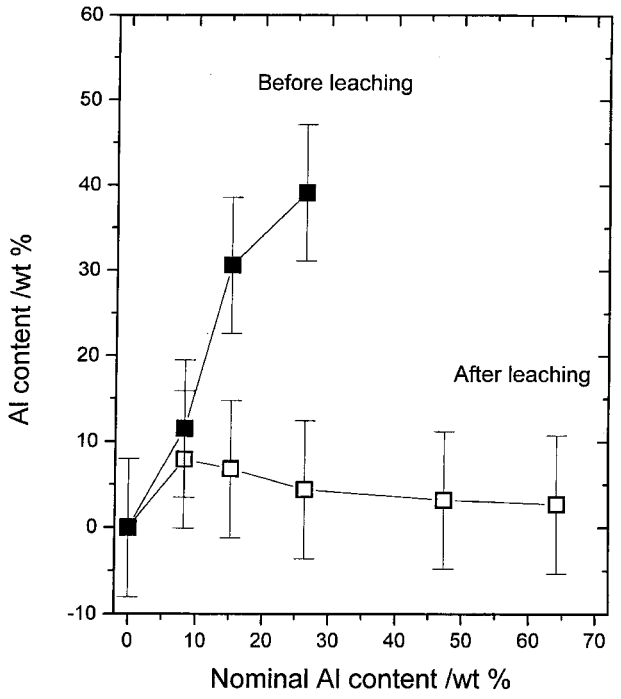

Fig. 6. Variation of the Al content before and after leaching with respect to the nominal Al composition, as monitored by EDX.

The morphology of powder before and after leaching is presented in Figure 7 for Ti:Ru:Fe:Al (3:1:1:1). Before leaching, the particles have dimensions slightly larger than 1 μm and they have relatively smooth surfaces (Fig. 7(a)). After leaching, the particles size distribution remains the same but the surfaces are highly porous (Fig. 7(b)). BET measurements performed on such powders indicate that there is a ten-fold increase in the specific surface area, from 0.7 $m^2\ g^{-1}$ to 7.0 $m^2\ g^{-1}$. The surface structure seen in Figure 7(b) closely resembled that of Raney nickel activated cathodes obtained after caustic leaching of $NiAl_3$ alloy [26].

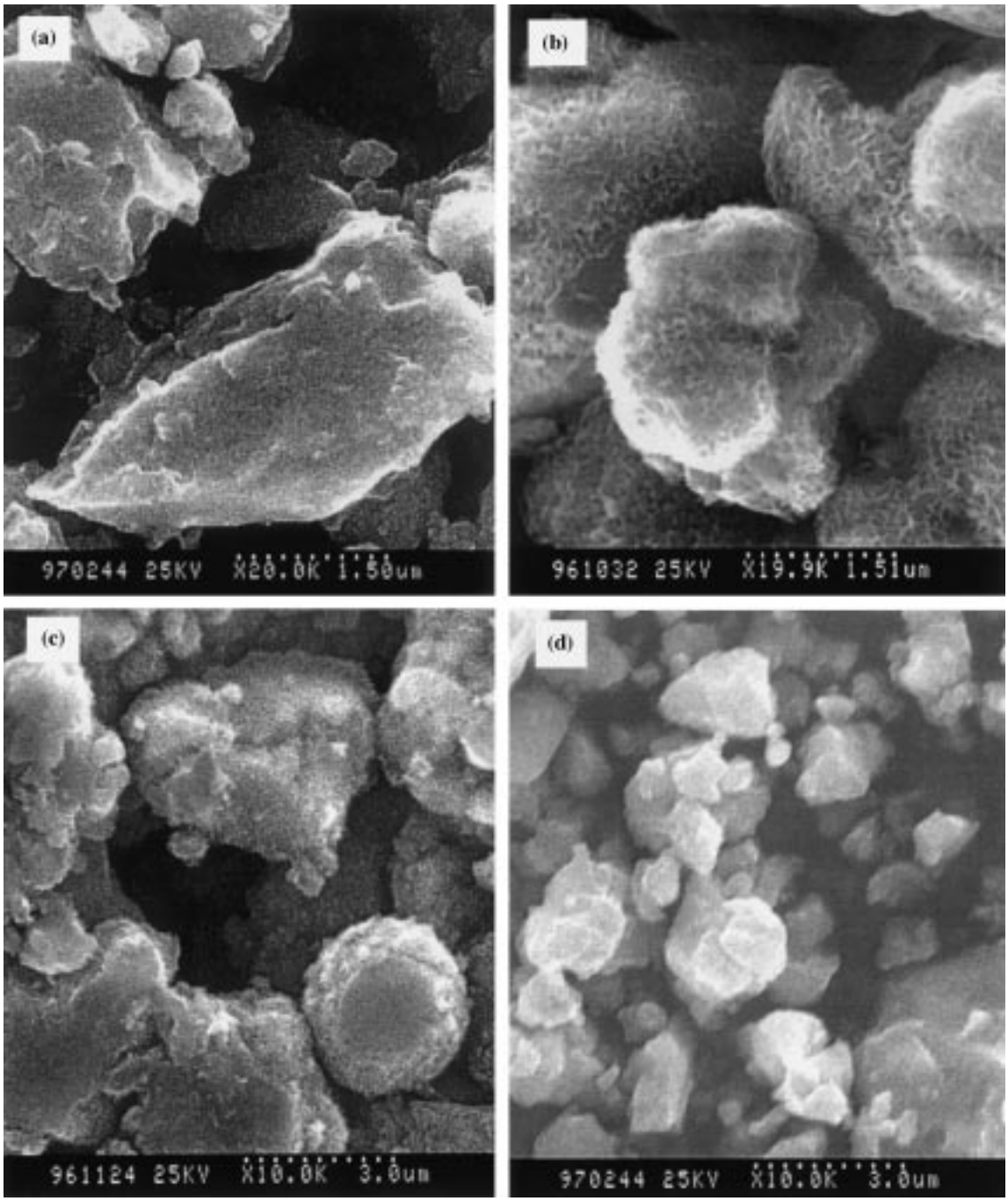

Fig. 7. SEM micrographs of preformed Ti:Ru:Fe (3:1:1) mixed with one equivalent of Al: (a) before leaching, (b) after leaching, (c) cold pressed electrode made of leached powder and (d) cold-pressed electrode made of remilled leached powder.

To monitor structural changes following leaching treatments, we took XRD spectra. Figure 8 shows patterns of Ti:Ru:Fe:Al (3:1:1:2) before and after lixiviation. The results indicate that the crystalline structure of the material stays the same and this has been the case for all samples. The absence of shift of the diffraction lines after lixiviation means that Al in solid solution in the cubic structure is not leached out during the treatment. This observation is confirmed by Rietveld analyses which show that there is no significant change in the lattice parameters after leaching (see Fig. 4). These results are consistent with the measurements of the Al content after leaching made by EDX analysis (Fig. 6).

3.3. *Electrochemical characterizations*

The electrochemical behaviour of electrodes were evaluated by chronopotentiometry. For all samples made with leached powders, the overpotential at 250 mA cm^{-2}, η_{250}, increases as the reaction proceeds. The increase of the overpotential over time is due to material decripitation and loss of structural integrity. Pieces of the electrode fall into the electrolyte during hydrogen evolution. After about 60 min of electrolysis, large parts of the top surface layer have been removed and the rate of change of η_{250} seems to level off. This behaviour differs markedly from that of Ti_3RuFe which exhibits a stable potential over the same time period. The η_{250} values at $t = 1$ min and $t = 60$ min are plotted in Figure 9 for various initial Al content. The overpotentials of the leached powders are 50 to 100 mV lower than that of the unleached material, probably because of the larger effective surface area. This hypothesis is consistent with the SEM micrograph of a cold pressed electrode made from leached powder (Fig. 7(c)), which shows the electrode material retains its porous structure after pressing. However, ways to prevent the decrepitation of the material and the loss of the structural integrity of the electrode have to be found in order to take advantage of the increased surface area.

The mechanisms of degradation of nanocrystalline Ti_2RuFe and the stabilization effect on the alloy by the introduction of oxygen has been discussed at length in previous papers from this laboratory [11, 27–30]. In the case of Ti_2RuFe, it is the hydriding–dehydriding cycles which occur during successive cathodic polarization and open-circuit conditions which are at the origin of the degradation [27, 28]. However, this effect occurs on a time scale of several hours and typically, Ti_2RuFe electrodes do not show any sign of deterioration before

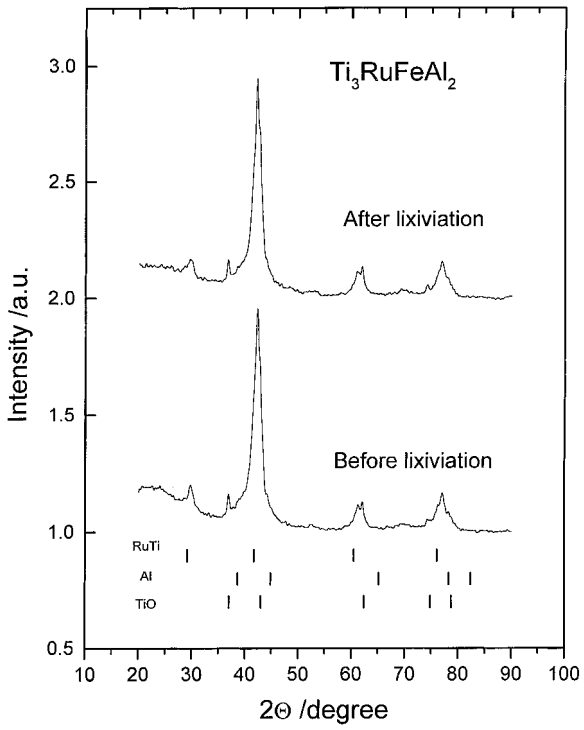

Fig. 8. XRD patterns of Ti–Ru–Fe–Al (3:1:1:2) before and after leaching.

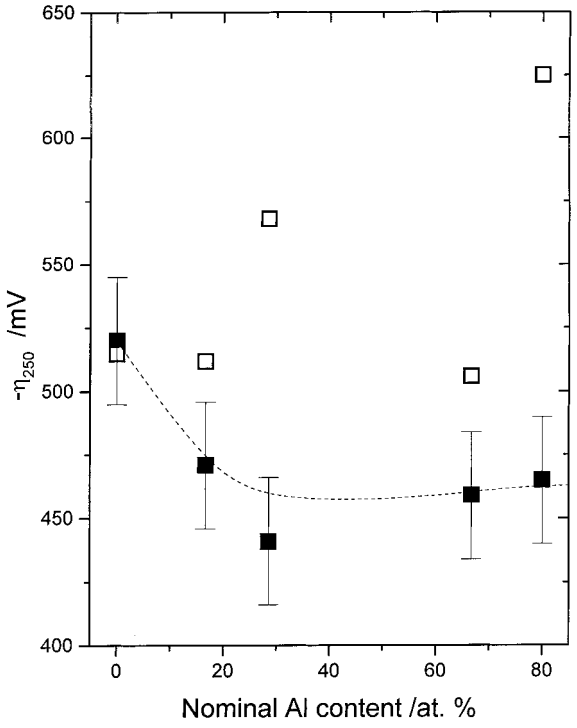

Fig. 9. Measured overpotentials at 250 mA cm^{-2} as a function of the nominal Al content. Key: (■) initial; (□) after 1 h.

100 h of electrolysis [11, 27]. In the case of the leached alloy, material decrepitation occurs on a time scale of a few minutes, much faster than for the mechanism described above, which suggest that a different phenomenon is at play.

The SEM micrograph of the cold-pressed electrode made from leached powder (Fig. 7(c)) suggests that the forces keeping the particles together are probably weak because of a reduced contact area between them. It is thus hypothesized that hydrogen gas bubbles that are formed during hydrogen discharge exerts a pressure large enough to cause the erosion of the porous surface and the decrepitation of the electrode.

An alternative hypothesis would be that the small amount of Al left in the cubic structure is leached out of the nanocrystalline alloy during the electrolysis test. These tests are conducted at 70 °C and the pH of the solution near the electrode can be quite high (pH 13–14) as a result of hydrogen discharge. In these conditions, Al found in the near surface region could dissolve and fragilize the assembly.

To test these two hypotheses, the leached powders were milled a second time. As shown by SEM (micrograph not shown), this milling step removes all the fine pores of the leached material. The morphology of the obtained powder resembles closely that of Figure 7(a). The cold-pressed electrode made from that powder (Fig. 7(d)) does not show any sign of deterioration over a period of one hour of electrolysis. Its catalytic activity however is greatly reduced to $\eta_{250} = 640$ mV. This confirms: (i) that the mechanical integrity of the electrode depends on the morphology of the leached powder and not on its chemical composition; and (ii) that the improvement of the global electrocatalytic activity is due to the large effective surface area of the leached powder.

Finally, several parameters of the electrode preparation procedure were varied, in an effort to increase the mechanical integrity of the electrode made from leached powder. Of these parameters, the most important is the temperature of the heat-treatment step of the leached powder prior to its use in the making of electrodes. Figure 10 shows a comparative short-term electrolysis test between Ti_3RuFe and the same material after lixiviation (one equivalent of Al). In the case of the leached material, there is no visual sign of degradation and the integrity of the electrode is maintained after this test. This situation differs greatly from the one observed previously, whereby pieces of the electrode made from as-leached powders were falling into the electrolyte. Compare to the unleached material, there is a reduction of the overpotential by about 50–80 mV. Most probably, the lost of hydration water molecules at the surface of the material leads to the formation of a more rigid layer which favors the mechanical anchoring between the particles.

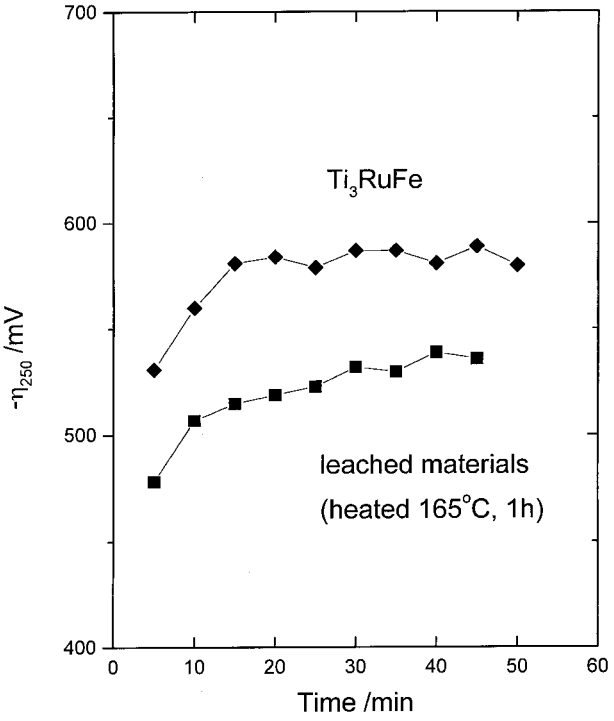

Fig. 10. Variation of η_{250} with time.

4. Conclusion

It was shown that inert atmosphere ball-milling could be used to prepared nanocrystalline Ti–Ru–Fe alloys with various Al content. The leaching process in the alkaline solution removes only the Al which is not in solid solution in the cubic structure of Ti_3RuFe. A highly porous surface structure, with a BET surface area ten times larger, is obtained after lixiviation. When used as activated cathode materials in typical chlorate electrolysis conditions, these leached powders reduce the cathodic overpotential by about 80 mV compared to that of unleached powders. High energy milling tools with large volume container are available on the market and, as far as we can judge, the process described above could be scaled up for the fabrication of large quantity of nanocrystalline Ti–Ru–Fe alloy with high specific surface area. It is expected that the extra reduction of the cathodic overpotential and the energy savings thus accomplished will overcome the cost associated with the few more steps involved in the powder preparation.

Acknowledgement

This work was supported by the Natural Sciences and Engineering Research Council of Canada and Hydro-Québec.

References

1. R. Birringer, *Mater. Sci. Eng.* **A117** (1989) 33.
2. O. El Kedim, M. Tachikart and E. Gaffet, *Mater. Sci. Forum* **225–227** (1996) 825.
3. L. Roué, M. Blouin, D. Guay and R. Schulz, *J. Electrochem. Soc.* **145** (1998) 1624.
4. J.Y. Huot, M.L. Trudeau and R. Schulz, *J. Electrochem. Soc.* **138** (1991) 1316.
5. R. Schulz, J.Y. Huot, M.L. Trudeau, L. Dignard-Bailey, Z.H. Yan, *J. Mater. Res.* **9** (1992) 2998.
6. R.W. Siegel, *Annual Rev. Mater. Sci.* **21** (1991) 559.
7. Yamashita, *J. Chem. Soc., Faraday Trans. II* **83** (1987) 2895.
8. Yoshizawa, *J. Appl. Phys.* **64** (1988) 6044.
9. H.J. Fecht, *in 'Advances in Powder Metallurgy'*, vol.2 (MPIF, Princeton, NJ, 1989), pp. 111–122.
10. M. Blouin, D. Guay, J. Huot and R. Schulz, *J. Mater. Res.* **12** (1997) 1492.
11. D. Guay, S.-H. Yip, É. Irissou, L. Roué, M. Blouin, S. Boily, J. Huot and R. Schulz, International Forum on 'Electrolysis in the Chemical Industry' (Electrosynthesis Co., Lancaster, NY: 1996), p. 346.
12. S.-H. Yip, D. Guay, S. Jin, E. Ghali, A. Van Neste and R. Schulz, *J. Mater. Res.* **13** (1998) 1171.
13. Th. Borucinsky, S. Rausch and H. Wendt, *J. Appl. Electrochem.* **27** (1997) 762.
14. R. Schulz, G. Lalande, J. Huot, M.-C . Denis, G. Liang, A. Van Neste, D. Guay and J.P. Dodelet, 'Leached nanocrystalline materials process for manufacture of the same , and use thereof in the energetic field' Patent pending.
15. J. Huot, S. Bouaricha, S. Boily, J.P. Dodelet , D. Guay and R. Schulz, *J. Alloys and Compounds* **266** (1998) 307.
16. F. Izumi, *in 'The Rietveld Method'*, edited by R. A. Young (Oxford University Press, Oxford, 1993), pp. 236–53.
17. Y.-I. Kim and F. Izumi, *J. Ceram. Soc. Jpn* **102** (1994) 401.
18. C. McCullough, J.J. Valencia, C.G. Levi and R. Mehrabian, *Acta Metall.* **37** (1989) 1321.
19. C. Suryanarayana, G.-H. Chen, A. Frefer and F.H. Froes, *Mat. Sci. Eng.* **A158** (1992) 93.
20. W. Guo, S. Martelli, N. Burgio, M. Magini, F. Padella and E. Paradisio, *J. Mater. Sci.* **26** (1990) 6190.
21. A.V. Leonov, E. Szewczak, O.E. Gladilina, H. Matyja, V.I. Fadeeva, *Mater. Sci. Forum* **235-238** (1997) 67.
22. G. Walkowiak, T. Sell and H. Mehrer, *Z. Metallkd.* **85** (1994) 332.
23. W. Guo, S. Martelli, F. Padella, M. Magini, N. Burgio, E. Paradisio and U. Franzoni, *Mater. Sci. Forum* **88–90** (1992) 139.
24. R. Ray, B.C. Giessen and N. Grant, *J. Metal. Trans.* **3** (1972) 627.
25. L. Zaluski, P. Tessier, D.H. Ryan, C.B. Doner, A. Zaluska, J.O. Ström-Olsen, M.L. Trudeau and R. Schulz, *J. Mater. Res.*, **8** (1993) 3059.
26. H. Wendt and V. Plzak, in 'Electrochemical Hydrogen Technologies: Electrochemical Production and Combustion of Hydrogen', edited by H. Wendt (Elsevier, Amsterdam, 1990), pp. 15–62.
27. L. Roué, É. Irissou, A. Bercier, S. Bouaricha, M. Blouin, D. Guay, S. Boily and R. Schulz, *J. Appl. Electrochem.* **29** (1999) 553.
28. L. Roué, D. Guay and R. Schulz, *J. Electroanal. Chem.* **455** (1998) 83.
29. M. Blouin, D. Guay and R. Schulz, submitted to *Nanostruct. Mater.* **10** (1998) 523.
30. M. Blouin, D. Guay, J. Huot, R. Schulz and I.P. Swainson, *Chem. Mater.* **10** (1998) 3492.
31. V.E. Raub and E.Z. Röschel, *Metallk.* **12** (1963) 455.